Characterization and control of pulse shapes in a doubly resonant synchronously pumped optical parametric oscillator

Joseph E. Schaar,*,† Jason S. Pelc,† Konstantin L. Vodopyanov, and Martin M. Fejer

E. L. Ginzton Laboratory, Stanford University, 450 Via Palou, Stanford, California 94305, USA

*Corresponding author: jschaar@stanford.edu

Received 7 June 2010; revised 18 July 2010; accepted 19 July 2010;
posted 20 July 2010 (Doc. ID 129354); published 11 August 2010

The intracavity signal and idler pulses of a low-loss synchronously pumped doubly resonant optical parametric oscillator were characterized experimentally and simulated numerically versus cavity-length detuning. At operation several hundreds of times above threshold, the detunings that maximize the intracavity average power do not necessarily maximize the temporal overlap of the signal and idler pulses, as is desirable for devices making use of intracavity mixing. Independent control of the signal and idler cavity lengths allowed control of the widths and temporal positioning of the pulses. Numerical studies were performed exploring the intracavity power and temporal overlap of the signal and idler pulses under various group-velocity-mismatch conditions. There was good agreement between the experimental and numerical simulation results. © 2010 Optical Society of America

OCIS codes: 190.4970, 190.7220.

Synchronously pumped optical parametric oscillators (SPOPOs) have become widely used sources of frequency-tunable high-peak-power light [1,2]. In addition to investigations of efficient frequency conversion, their use has spread to the fields of spectroscopy [3], nonlinear microscopy [4], and frequency-comb generation [5]. A large portion of the research studying SPOPOs has focused on the singly resonant case due to the stability of operation. Doubly resonant oscillators (DROs) resonate both the signal and idler waves, which lowers the threshold but requires strict control of the cavity length to achieve stable operation [6]. To the extent that the intracavity pulses can be controlled and optimized, the additional stored energy resulting from doubly resonant operation can significantly enhance the efficiency of intracavity parametric processes, such as terahertz (THz) generation via difference-frequency generation of the signal and idler pulses [7]. Theoretical investigations of singly resonant SPOPOs have been performed [8] but are only valid near threshold and have not been extended to the doubly resonant case.

We present experimental and numerical results on a synchronously pumped DRO that has been used for intracavity generation of tunable THz radiation [7,9]. A set of numerical simulation tools was developed to calculate the temporal behavior of the synchronously pumped DRO. We find that the cavity-length detunings of the signal and idler cavities are important parameters governing the behavior of the system. In this paper, we demonstrate that the signal and idler pulse shapes and relative temporal positioning can be controlled as the cavity-length detunings are varied. We found that certain cavity-length detuning configurations, as governed by the relative group-velocity-mismatch (GVM) conditions of the three interacting waves, are optimal for maximizing the temporal overlap of the signal and idler. We also identified cavity-length detuning regions where oscillation is not allowed due to backconversion of the signal and idler photons to pump photons.

A schematic of the experimental setup is shown in Fig. 1. The 6 m long (round trip) OPO cavity was

0003-6935/10/244489-05$15.00/0

pumped by a 1064 nm mode-locked laser with a Fourier-transform-limited pulse duration $\tau_p = 8$ ps (Gaussian $1/e^2$ intensity half-width) and repetition rate $f_{\text{rep}} = 50$ MHz. The OPO gain medium was a 10 mm long periodically poled magnesium-doped lithium niobate (PPMgLN) crystal designed for Type II quasi-phase-matching (QPM) ($\Lambda_g = 14.1$ μm) so that the signal and idler fields were orthogonally polarized. The mode-matching optics (MMO) created a pump beam spot size of 30 μm at the center of the PPMgLN crystal, and the signal and idler beam spot sizes were 57 μm. The signal and idler frequencies were tuned to a frequency difference of 1.5 THz by setting the crystal temperature at 85 °C, where $\omega_p > \omega_s > \omega_i$ and p, s, and i correspond to pump, signal, and idler, respectively. Additional details of the SPOPO cavity can be found in [7].

This staggered-cavity design allowed independent control of the signal and idler cavity lengths, L_s and L_i, leading to control of the relative timing of the signal and idler pulses. Mirrors M2 and M4 were mounted on motorized translation stages that controlled the signal and idler cavity lengths, respectively. The motorized displacements of M2 and M4 introduce round-trip cavity-length detunings, ΔL_s and ΔL_i, respectively. We define the cavity lengths that minimize the DRO threshold power as L_{0s} and L_{0i}, where, by definition, $\Delta L_s = \Delta L_i = 0$, and we define detunings according to $\Delta L_s = L_s - L_{0s}$ and $\Delta L_i = L_i - L_{0i}$. We define normalized temporal delays for the signal and idler pulses as $\Delta \bar{T}_s = \Delta L_s/(c\tau_p)$ and $\Delta \bar{T}_i = \Delta L_i/(c\tau_p)$, respectively.

We performed numerical simulations where propagation through the PPMgLN crystal is calculated using a symmetric split-step Fourier method [10,11] that includes three-wave mixing, group-velocity mismatch (GVM), group-velocity dispersion, self-phase modulation (SPM), and cross-phase modulation (XPM). The physical effects mainly responsible for the relative timing and shapes of the signal and idler pulses for this OPO were three-wave mixing and GVM. The room-temperature dispersion information for PPMgLN was taken from [12], with temperature-dependent coefficients taken from [13]. The nonlinear optical coefficient for Type II QPM at 2.1 μm is $d_{31,\text{eff}} = 2.35$ pm/V [7]. In a method similar to that used in [14] for resonant second-harmonic

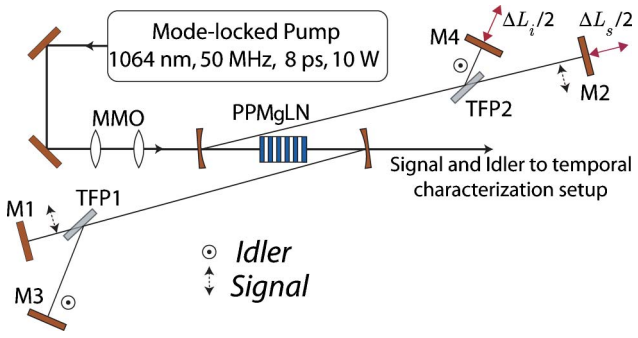

Fig. 1. (Color online) Experimental setup of the doubly resonant SPOPO. TFP, thin film polarizer; MMO, mode-matching optics.

generation, we assumed the three waves to be Gaussian TEM_{00} modes and derived position-dependent complex corrections to both the second- and third-order nonlinear coupling terms assuming the transverse mode shapes do not change. A value of $\chi^{(3)} = 1.43 \times 10^{-21}$ m^2/V^2 was assumed for the third-order nonlinear susceptibilities [15]. We extended the simulation method used in [10] for two resonating waves; the buildup of the OPO was simulated until steady-state pulses were reached, which typically takes of the order of 100 round trips. Such simulations were performed over a wide range of ΔL_s and ΔL_i.

The DRO was designed to generate large intracavity signal and idler powers in order to efficiently generate THz radiation within an orientation-patterned GaAs crystal placed inside the cavity. Therefore, a second requirement was to configure the DRO such that the temporal overlap of the intracavity signal and idler pulses is large. To experimentally measure the temporal overlap of the signal and idler pulses, extracavity sum-frequency generation (SFG) between the signal and idler was performed in a 5 mm long PPMgLN crystal. Additionally, we used the same crystal for characterization of the signal and idler pulse shapes and temporal positioning. Using a delay stage for the pump pulses, we measured intensity cross correlations of the signal and idler pulses with the pump pulses by an SFG process generating red pulses with $\lambda \sim 700$ nm.

The sum of the signal and idler intracavity average powers P_{tot} was experimentally monitored as $\Delta \bar{T}_s$ and $\Delta \bar{T}_i$ were scanned between –0.8 and 0.8, creating a "detuning map" [Fig. 2(a)]. The minimized DRO threshold was 50 mW, corresponding to the origin of Fig. 2. At a pump power of 9 W, oscillation was observed in quadrants II and IV [Fig. 2(a)], where the signal and idler were detuned in opposite directions and $P_{\text{tot}} \sim 100$ W. Oscillation was observed in quadrants I and III for $|\Delta \bar{T}| < 0.05$.

We find that the temporal overlap of the signal and idler was maximized in quadrant II [Fig. 2(c)]. Since the idler group velocity is larger than the signal group velocity within the PPMgLN crystal ($u_i = 0.46c$, $u_s = 0.443c$, and $u_p = 0.436c$), the temporal overlap of the intracavity pulses after the crystal was largest when the idler lagged the signal before entering the crystal (i.e., $\Delta \bar{T}_i > 0$, $\Delta \bar{T}_s < 0$), such that the idler pulse catches up to the signal as the pulses propagate through the PPMgLN crystal. Operation in quadrant IV yields a lower temporal overlap because the signal and idler pulses walk off as they propagate through the PPMgLN crystal. The phase-matched signal and idler wavelengths tuned slightly, as well as the corresponding signal and idler group velocities within the PPMgLN crystal, to ensure synchronicity with the pump pulses as the cavity lengths varied. This wavelength tuning was small ($\Delta\lambda_s$, $\Delta\lambda_i < 3$ nm) compared to the full width at half-maximum bandwidth of the high-reflectance coating

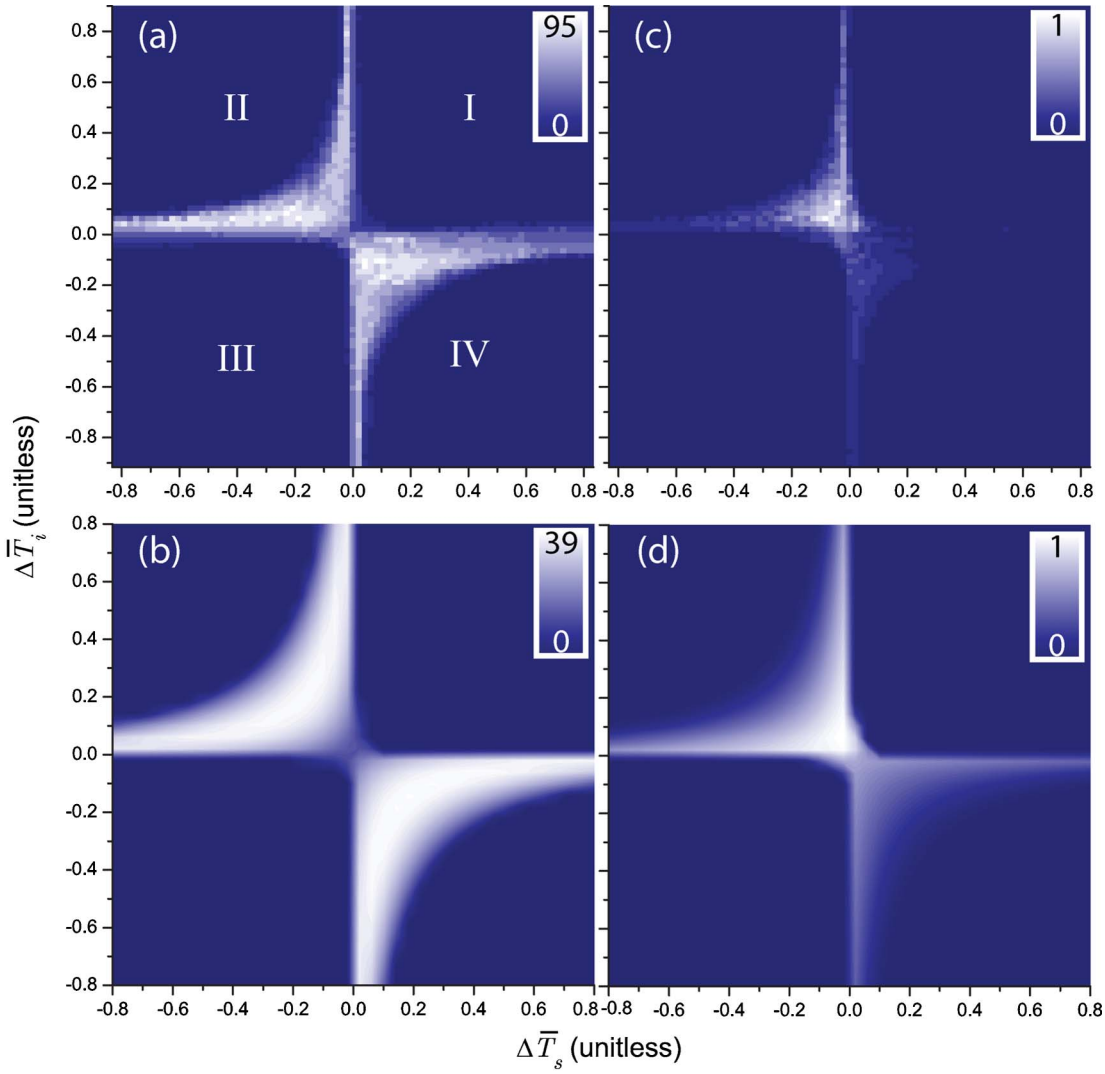

Fig. 2. (Color online) (a) Experimental and (b) numerically calculated results for P_{tot} at constant times above threshold. (c) Experimental and (d) numerically calculated results for extracavity signal + idler SFG, with the maximum SFG values normalized to unity.

of the cavity mirrors, $\Delta\lambda = 500$ nm at an average wavelength of 2128 nm.

The DRO threshold calculated by the numerical simulations was 10 mW. Measurement of the threshold of the synchronously pumped DRO involved optimizing the signal cavity length to maximize the DRO power while dithering the idler cavity length approximately 4 μm, corresponding to approximately four cavity fringes. Because of the slow buildup time of the OPO near threshold (0.1–1 ms), it was difficult to accurately determine the oscillation threshold using standard length-dithering techniques. The simulations were performed at a pump power of 1.8 W instead of 9 W such that the plots are for constant times above threshold. The results of the numerical simulation are plotted in Figs. 2(b) and 2(d), and we find good agreement between the experimental and simulated results. The different maximum values in Figs. 2(a) and 2(b) of 95 and 39 W, respectively, are due to the different absolute pumping levels. The largest values in Figs. 2(c) and 2(d) are normalized to unity.

In Figs. 3(a) and 3(b), we plot experimentally measured and numerically calculated intensity cross correlations of the signal and idler pulses with the pump pulse (red-SFG). The signal and idler pulse widths can be substantially longer than the pump pulse ($\tau_p = 8$ ps) due to nonzero detunings, low loss, and operation many times above threshold [8,16]. Figure 3(a) plots the experimentally measured (circles and squares) and numerically calculated (solid and dashed curves) signal and idler cross correlations with the pump, respectively, with the peak intensities normalized to unity. The normalized detunings for the experiment and simulation were $\Delta\bar{T}_s = -0.18$ and $\Delta\bar{T}_i = 0.1$. This corresponds to a point in quadrant II of the detuning map where the temporal overlap is large. Also, the signal pulse leads the idler pulse as expected, given the signs of $\Delta\bar{T}_s$ and $\Delta\bar{T}_i$. Figure 3(b) plots experimental and

numerical data at a point in quadrant IV where the intracavity power is large, but the temporal overlap is small. The normalized detunings were $\Delta\bar{T}_s = 0.17$ and $\Delta\bar{T}_i = -0.1$. The idler pulse leads the signal pulse, again in agreement with the signs of the detunings, and the temporal overlap in Fig. 3(b) is smaller than that of Fig. 3(a). Since the signal and idler detunings have opposite signs, the tails of the signal and idler pulses extend in opposite directions. The steady-state pulse shapes result from a cycle, which repeats every round trip, where the cavity-length detunings temporally separate the signal and idler pulses, but the three-wave mixing with the pump in the PPMgLN amplifies the pulses near $t = 0$, when all three pulses temporally overlap, bringing the pulses closer together. The relative temporal positioning and temporal overlap of the intracavity signal and idler pulses can be controlled by varying ΔL_s and ΔL_i.

Simulations where the group indices were varied showed that the quadrant with the largest temporal overlap had opposite signs for the two quantities $(n_{gs} - n_{gi})$ and $(\Delta\bar{T}_s - \Delta\bar{T}_i)$, where n_{gs} and n_{gi} are the group indices of the signal and idler, respectively. The detunings counteracted temporal walk-off between the signal and idler pulses such that the overlap was maximized upon exiting the PPMgLN crystal.

At particular cavity-length detunings, fluctuations in the signal and idler average powers were observed. The fluctuations can be microsecond-scale transients or periodic fluctuations (100–500 kHz), depending on the cavity-length detunings. The numerical calculations suggest that the fluctuations are the result of the combined effects of three-wave mixing, GVM, SPM, and XPM in the PPMgLN crystal. To eliminate the fluctuations, the round-trip nonlinear phase accumulated by the signal and idler fields [17] should roughly be less than the cavity loss times π [18].

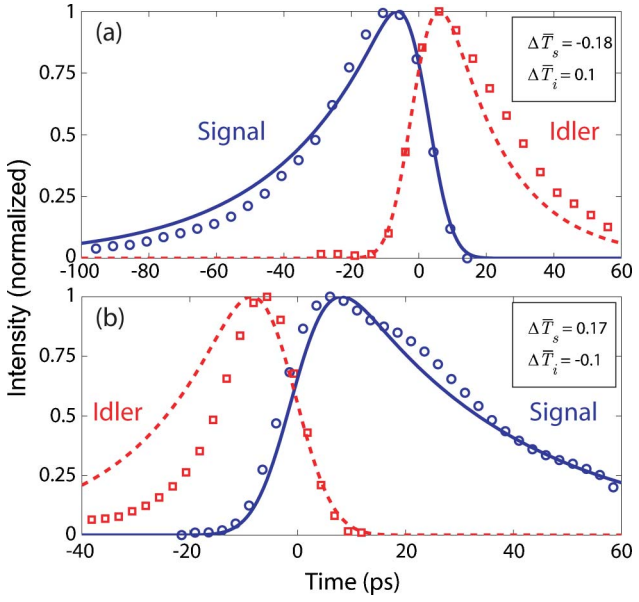

Fig. 3. (Color online) Signal and idler measured (circles and squares) and numerically calculated (solid and dashed curves) cross correlations with the pump for a detuning in (a) quadrant II and (b) quadrant IV of Fig. 2. The maximum intensities are normalized to unity.

Additional numerical simulations showed that operating 2–4 times above threshold allowed for large temporal overlap of the signal and idler pulses, which were also comparable in width to the pump pulse. Decreasing the gain of the SPOPO results in operation closer to threshold. For a set pump power and set pump, signal, and idler beam spot sizes, the gain can be decreased by decreasing the length of the PPMgLN crystal. Analysis of the temporal overlap of the signal and idler pulses versus times above threshold is the focus of a future investigation.

The widths and temporal positioning of the intracavity signal and idler pulses of a low-loss synchronously pumped DRO were characterized versus cavity-length detuning experimentally and numerically. In cases pumped several hundreds of times above threshold, the DRO produced signal and idler pulses that were substantially longer than the pump pulse. It was found that, in this highly over-pumped case, the cavity-length detunings that maximized the intracavity average power did not necessarily maximize the temporal overlap of the signal and idler pulses, and that the signal and idler cavity-length detunings determined the temporal positioning of the pulses. There was good agreement between the experimental and numerical simulation results. It was determined that temporal overlap of signal and idler pulses was maximized when cavity-length detuning counteracted temporal walk-off between the signal and idler pulses in the DRO gain medium.

[†]Contributed equally to this work.

References

1. E. C. Cheung, K. Koch, and G. T. Moore, "Frequency upconversion by phase-matched sum-frequency generation in an optical parametric oscillator," Opt. Lett. **19**, 1967–1969 (1994).
2. M. E. Dearborn, K. Koch, G. T. Moore, and J. C. Diels, "Greater than 100% photon-conversion efficiency from an optical parametric oscillator with intracavity difference-frequency mixing," Opt. Lett. **23**, 759–761 (1998).
3. K. A. Tillman, R. R. J. Maier, D. T. Reid, and E. D. McNaghten, "Mid-infrared absorption spectroscopy of methane using a broadband femtosecond optical parametric oscillator based on aperiodically poled lithium niobate," J. Opt. A Pure Appl. Opt. **7**, S408–S414 (2005).
4. G. McConnell, "Nonlinear optical microscopy at wavelengths exceeding 1.4 μm using a synchronously pumped femtosecond-pulsed optical parametric oscillator," Phys. Med. Biol. **52**, 717–724 (2007).
5. J. H. Sun, B. J. S. Gale, and D. T. Reid, "Composite frequency comb spanning 0.4–2.4 μm from a phase-controlled femtosecond Ti:sapphire laser and synchronously pumped optical parametric oscillator," Opt. Lett. **32**, 1414–1416 (2007).
6. J. Falk, "Instabilities in the doubly resonant parametric oscillator: a theoretical analysis," IEEE J. Quantum Electron. **7**, 230–235 (1971).
7. J. E. Schaar, K. L. Vodopyanov, P. S. Kuo, M. M. Fejer, A. Lin, J. S. Harris, D. Bliss, C. Lynch, V. G. Kozlov, and W. Hurlbut,

"Terahertz sources based on intracavity parametric down-conversion in quasi-phase-matched gallium arsenide," IEEE J. Sel. Top. Quantum Electron. **14**, 354–362 (2008).
8. E. C. Cheung and J. M. Liu, "Theory of a synchronously pumped optical parametric oscillator in steady-state operation," J. Opt. Soc. Am. B **7**, 1385–1401 (1990).
9. J. E. Schaar, K. L. Vodopyanov, and M. M. Fejer, "Intracavity terahertz-wave generation in a synchronously pumped optical parametric oscillator using quasi-phase-matched GaAs," Opt. Lett. **32**, 1284–1286 (2007).
10. B. Ruffing, A. Nebel, and R. Wallenstein, "All-solid-state cw mode-locked picosecond $KTiOAsO_4$ (KTA) optical parametric oscillator," Appl. Phys. B **67**, 537–544 (1998).
11. G. P. Agrawal, *Nonlinear Fiber Optics*, 3rd ed. (Academic, 2001).
12. D. E. Zelmon, D. L. Small, and D. Jundt, "Infrared corrected Sellmeier coefficients for congruently grown lithium niobate and 5 mol.% magnesium oxide-doped lithium niobate," J. Opt. Soc. Am. B **14**, 3319–3322 (1997).
13. A. L. Aleksandrovskii, G. I. Ershova, G. Kh. Kitaeva, S. P. Kulik, I. I. Naumova, and V. V. Tarasenko, "Dispersion of the refractive indices of $LiNbO_3$:Mg and $LiNbO_3$:Y crystals," Sov. J. Quantum Electron. **21**, 225–227 (1991).
14. S. Schiller, "Principles and applications of optical monolithic total-internal-reflection resonators," Ph.D. dissertation (Stanford University, 1993).
15. R. DeSalvo, A. A. Said, D. J. Hagan, E. W. Van Stryland, and M. Sheik-Bahae, "Infrared to ultraviolet measurements of two-photon absorption and n_2 in wide bandgap solids," IEEE J. Quantum Electron. **32**, 1324–1333 (1996).
16. A. Haché, G. R. Allan, and H. M. van Driel, "Effects of cavity detuning on the pulse characteristics of a femtosecond synchronously pumped optical parametric oscillator," J. Opt. Soc. Am. B **12**, 2209–2213 (1995).
17. A. E. Siegman, *Lasers* (University Science, 1986).
18. J. E. Schaar, "Terahertz sources based on intracavity parametric frequency down-conversion using quasi-phase-matched gallium arsenide," Ph.D. dissertation (Stanford University, 2009).